May 14-17, 2007, Montreal, Canada

GT2007-27020

LOCAL COOLING EFFECTIVENESS DISTRIBUTION OF AN INTEGRATED IMPINGEMENT AND PIN FIN COOLING CONFIGURATION

Chiyuki Nakamata
Ishikawajima-Harima Heavy Industries Co., Ltd. Aero-Engine & Space Operations
TOKYO 190-1297 JAPAN
E-mail: chiyuki_nakamata@ihi.co.jp

Fujio Mimura, Masahiro Matsushita, Takashi Yamane, Yoshitaka Fukuyama
Japan Aerospace Exploration Agency
Tokyo 182-8522 JAPAN

Toyoaki Yoshida
Tokyo University of Agriculture and Technology
Tokyo 184-8588 JAPAN

ABSTRACT

An integrated impingement and pin-fin cooling configuration is investigated experimentally. Temperature measurements have been performed for several test pieces with various pin/hole arrangements to clarify an influence of pin/hole arrangements on cooling effectiveness. The experiment has been conducted with 673K combustion gas flow and room temperature cooling air. Reynolds number of combustion gas flow is 380000 and Reynolds number of cooling air flow is in the range from 5000 to 30000. An infrared camera is used to measure a temperature distribution on a specimen surface. The area-averaged cooling effectiveness and the local cooling effectiveness are evaluated for each specimen and compared each other. There are evidences of the existence of pins on the local cooling effectiveness at the exact location of those. But the local cooling effectiveness are independent of the hole arrangement.

Keywords: impingement cooling,
heat transfer enhancement,
film cooling,
pin fin,
cooling effectiveness

INTRODUCTION

To meet a demand for higher turbine inlet temperature (TIT) in aero-engines or gas turbines with minimum cooling air flow, there is a great need to develop a revolutionary new cooling system for high-pressure turbine stages. This demand motivates many researchers to develop a high performance cooling configuration. As a result, many advanced cooling configurations based on a double wall cooling configuration have been developed for several decades, and they are still attractive research objects. An impingement/effusion cooling (Andrews et al. [13], Al Dabagh et al. [14], Cho et al. [15, 16], Zhang et al. [6]) and an impingement cooling with surface enlargement elements (Trabold et al. [8], Haiping et al. [9], Hoecker et al. [10], Annerfeldt et al. [11], Andrews et al. [12]) have been developed since the latter half of 80's. And, several advanced double wall cooling configurations with surface enlargement elements have been developed in 90's. Some examples are an integrally cast cooling (Gillespie et al. [1], Chambers et al.[19], Ieronymidis et al. [20-22]), Lamilloy® (Sweeney et al. [2]), an advanced leading edge impingement cooling concept (Taslim et al. [3]), an integrated impingement and pin fin cooling configuration (Funazaki et al. [4], Yamawaki et al. [17], Favaretto et al. [18], Nakamata et al. [5]), an in-wall mesh cooling technique (Bunker et al. [7]), and an advanced double-wall cooling system developed by AVIO (Coutandin et al. [24]). One of the most important technologies to realize a complicated double wall cooling configuration in an actual engine is a manufacturing technology. An electroforming based technology called Poroform® that is intended to be applied to a manufacture of an effusion-cooled turbine blade is investigated by Battisti et al. [23]. The manufacturing technique and the result of the computational feasibility study have been reported. Poroform® is considered to have a possibility to make a fine structure even though the cooling configuration studied by Battisti et al. [23] is not a double wall configuration.

An integrated impingement and pin fin cooling configuration is a subject of this study. A conceptual drawing of the configuration is shown in Figure 1. It integrates an

impingement cooling and pin cooling devices into one body in order to enhance the effective cooling area of an impingement cooling. Published papers concerned with impingement and pin cooling are described in the following paragraphs.

Funazaki et al. [4] have reported the first research result for the integrated impingement and pin-fin cooling configuration. They have performed experimental and numerical researches on a heat transfer coefficient distribution inside the configuration. They have studied the most basic configuration that have one pin in an area that is bounded with one pitch of impingement and film cooling holes. It is found that an average heat transfer coefficient on the pin surface is almost the same as that on the target surface for $Z/d < 1.5$. Thus it is indicated that the cooling configuration has a great potential to realize ultra-high temperature turbine nozzle vanes with less cooling air consumption.

Yamawaki et al. [17] have evaluated an improvement of cooling effectiveness that is achieved by increasing a pin density in the configuration. Two specimens that have different pin densities (sectional area ratio of pins: $(\pi d_p^2 N_p)/(2X_p Y_p)$) are tested. The hot gas side surface temperatures of the specimens have been measured in a hot wind tunnel. It is found that the cooling effectiveness of a coarse pin density configuration agrees well with a simple prediction using a theoretical fin efficiency to estimate a coolant side area enhancement. On the other hand, the cooling effectiveness of a fine pin density configuration falls below the prediction. CFD analyses have been also performed to help an understanding of the experimental results mentioned above. The CFD results show that the pins in the fine pin density configuration narrow a high heat transfer region near the stagnation of the impingement by obstructing a spread of the impingement jet. This result indicates that the cooling effectiveness may be influenced by a pin arrangement.

Subsequently, Nakamata et al. [5] have performed another experimental study to clarify an effect of a spatial arrangement of pins and holes on a cooling performance of the integrated impingement and pin fin cooling configuration. Experimental results of three different configurations are described. An interesting result is obtained that the cooling effectiveness depends on the pin arrangement under the constant pin density condition. Thus the result suggests that a pin/hole arrangement is an important parameter as well as a pin density.

Only an area-averaged cooling effectiveness is evaluated in the paper of Nakamata et al. [5]. However a local cooling effectiveness must be evaluated to obtain a better knowledge about the pin arrangement effect on cooling effectiveness. Thus authors evaluate local cooling effectiveness to the existing experimental data that have been obtained through the study of Nakamata et al. [5]. This paper first describes detailed local cooling effectiveness for several cooling configurations that have different pin/hole arrangements to clarify an influence of the pin/hole arrangement on a local cooling effectiveness distribution.

NOMENCLATURE

A surface area in each unit area [m^2]
A_{surf} main stream side heat transfer surface area of a specimen

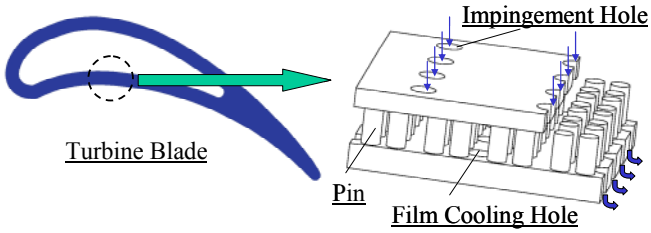

Figure 1 Concept of integrated impingement and pin fin cooling configuration

Cp Specific heat [J/(kgK)]
d diameter [m]
h heat transfer coefficient [W/(m^2K)]
L specimen length along gas flow [m]
M_i blowing ratio $=(\rho_c V_i)/(\rho V)_g$ based on impingement flow
N number
R geometric cooling side surface area ratio, Eq.(1)
Re_g Reynolds number of combustion gas flow$=V_g L/\nu$
Re_c Reynolds number of cooling air flow $=V_i d_i/\nu$
T temperature [K]
V mean velocity [m/s]
W mass flow rate [kg/s]
X_p row-to-row spacing of hole [m]
Y_p hole-to-hole pitch within row of hole [m]
Z pin height, impingement gap [m]
ν kinematic viscosity [m^2/s]
ρ density [kg/m^3]
η cooling effectiveness, Eq.(2)

Subscripts

c cooling air flow side, cooling air
f film cooling hole
g gas flow side, or gas
i impingement plate, or impingement flow or hole
in inlet of impingement hole
p pin
t target
w gas side wall

EXPERIMENTAL FACILITY AND TECNIQUES

The experiment has been conducted in a hot wind tunnel at the Japan Aerospace Exploration Agency. Figure 2 shows a schematic layout of the facility. The wind tunnel has a two-stage combustor that supplies high-temperature combustion gas to a test section. Cooling air is supplied through a bypass line that has an electric heater to control an air temperature. Inlet valves regulate both flow rates with measuring pressures of orifices. A pressure of the combustion gas in a test section is set by an exhaust valve located downstream of an exhaust cooler that has water injections. Figure 3 shows the test section in detail. A specimen is embedded on a rectangular combustion gas flow passage. The passage is the circle of 106mm in diameter at the combustor exit, and it is transformed into the rectangle of 40mm in height × 106mm in width at the upstream end of a specimen. This shrinkage of the passage in height makes flat distributions of a combustion gas temperature and a velocity above a specimen surface. To avoid a heat loss and keep constant a combustion

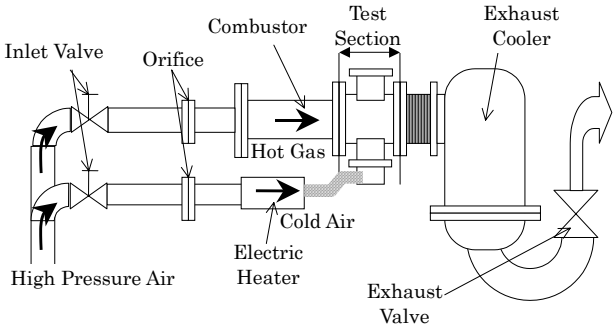

Figure 2 Schematic layout of hot wind tunnel

gas temperature in the test section, low-conductivity ceramic material Al_2O_3 is cast on an inner surface of the water-cooled outer duct. The gas passage is constructed of Al_2O_3-TiO_2 which is better than Al_2O_3 in a thermal shock resistance. A window is located on an opposite side of a specimen for IR camera measurement. High infrared transmissive ZnSe glass is used for the window. Combustion gas temperatures are measured at the inlet of the test section by two sheath thermocouple probes. The temperatures are measured near the center of the passage. A temperature difference between the measurements is within 2K. Cooling air temperatures are measured at two points near a specimen to account for pre-heating in the air cavity.

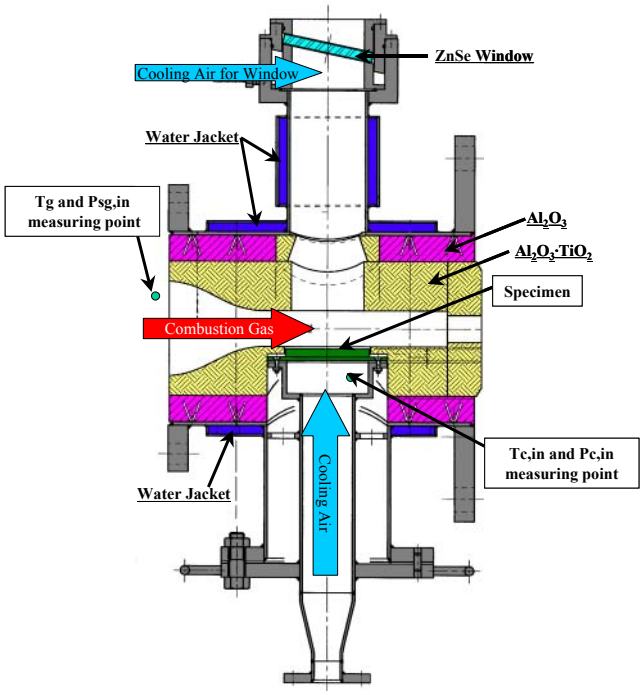

Figure 3 Test section detail

Specimens

Table 1 shows specimens. Figure 4 shows a schematic sectional view of one of the specimens with pins. All specimens have an impingement plate and a target plate. A distance between the plates is designed for a spacing of 6mm (Z/d_i=1.5), that is equal to an impingement gap. The impingement plate has impingement cooling holes. Diameters of the holes are 4mm. A periodic pattern of an arrangement of the impingement holes is shown in Figure 5. The row-to-row spacing of the holes is X_p=20mm. The hole-to-hole pitch in each row is Y_p=10mm. The non-dimensional spacing and pitch based on the impingement hole diameter of d_i=4mm are X_p/d_i=5.0 and Y_p/d_i=2.5, respectively.

Three specimens have no pin. They are Reference (REF), Conventional-Staggered (CSTAG) and Conventional-Shifted (CSHIFT). They are made of stainless steel.

REF has no pin, and no film cooling hole. It has only impingement cooling holes.

CSTAG has film cooling holes of 4mm in diameter in a target plate. And the film cooling holes are arranged to make the periodic pattern shown in Figure 5. To consider a configuration two-dimensionally by projecting a configuration on XY plane makes easy to explain a configuration. Thus explanations about relative locations of pins and holes are explained considering a two-dimensional configuration in the following paragraphs. A distance from a film cooling hole to the nearest impingement cooling hole is a half of the spacing in X direction and a half of the pitch in Y direction in the configuration of CSTAG.

CSHIFT also has film cooling holes of 4mm in diameter which are arranged to make the periodic pattern shown in Figure 5. A distance from a film cooling hole to the nearest impingement cooling hole is a half of the spacing in X direction and 0 in Y direction.

The other three specimens have configurations with pins. They are manufactured by casting with rapid prototyping cores, and they are made of Ni alloy. They are Basic (BASI), Staggered (STAG) and Staggered2 (STAG2).

BASI has the same size holes (d_i=d_f=4mm) at the same locations as CSHIFT, and it also has a pin of 4mm in diameter at each center of a half of the unit area one by one. A half of the unit area means a square that its four apexes are located at centers of four holes that are the nearest two impingement holes and two film cooling holes.

STAG has the same size holes (d_i=d_f=4mm) at the same locations as CSTAG. It also has three pins of 2.5mm in diameter in the unit area of 20mm × 10mm.

STAG2 has the same arrangement of holes and pins as an upside down configuration of STAG. Thus STAG and STAG2 are different in the pin arrangement although they have same pin densities.

BASI, STAG and STAG2 are examined by X-ray inspections. There are not defects in the internal structures of the specimens. The pin diameters are measured on the radiographs. And it is estimated that the pin diameters are correct within a 20% error. An amount of a change of cooling effectiveness that is generated by the pin diameter error is estimated by a one dimensional heat conduction analysis. An amount of the change is estimated 1.7%.

Two different materials are used to manufacture the specimens, as mentioned before. Thermal conductivities of stainless steel and Ni alloy are about 17W/m/K and about 10W/m/K on the test condition, respectively. An amount of a change of cooling effectiveness that is generated by the difference of the thermal conductivity is estimated by the one dimensional thermal conduction analysis, and cooling

Table 1 Specimens

		REF	CSHIFT	CSTAG
Outlook *Upstream: Left *Hole: Film hole			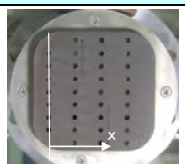	
Pin/Hole Arrangement *not scale ○ Film(ϕ4mm) ▨ Impingement(ϕ4mm)		 Unit:20mm x 10mm	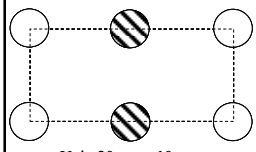 Unit:20mm x 10mm	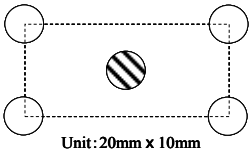 Unit:20mm x 10mm
Number	**Impingement**	**34**	**34**	**34**
	Film	**0**	**34**	**32**
Material		**Stainless Steel**		
		BASI	**STAG**	**STAG2**
Outlook *Upstream: Left *Hole: Film hole				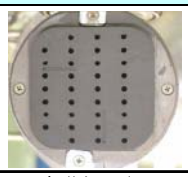
Pin/Hole Arrangement *not scale ○ Film(ϕ4mm) ▨ Impingement(ϕ4mm) ● Pin		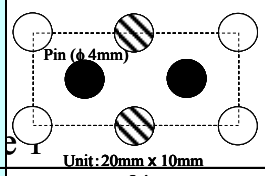 Pin (ϕ 4mm) Unit:20mm x 10mm	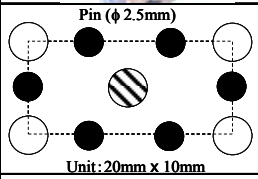 Pin (ϕ 2.5mm) Unit:20mm x 10mm	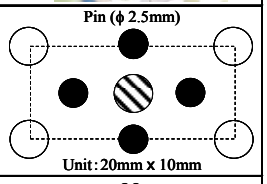 Pin (ϕ 2.5mm) Unit:20mm x 10mm
Number	**Impingement**	**34**	**34**	**32**
	Film	**34**	**32**	**34**
Material		**Nickel Alloy**		

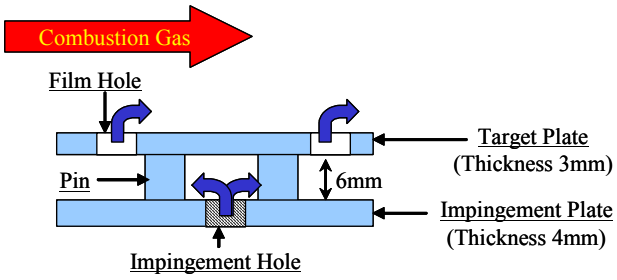

Figure 4 Schematic sectional view of specimen

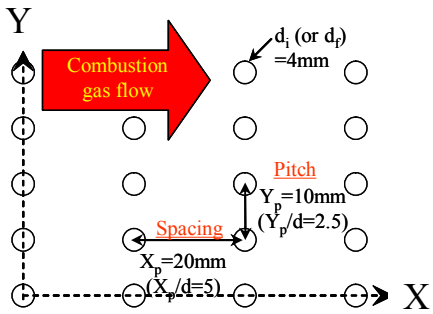

Figure 5 Impingement and film cooling hole arrangement pattern on each plane

effectiveness of the stainless steel specimens are corrected. It is 1-2% that cooling effectiveness of the stainless steel specimens are corrected.

A geometric cooling side surface area ratio, R, is defined as below,

$$R = \frac{(A_t + A_p)}{X_p \times Y_p} \quad (1)$$

R for BASI, STAG and STAG2 are 1.63.

All specimen surfaces are coated with a high-temperature black paint to maintain uniform and high emissivity on the surfaces.

IR camera calibration

An IR camera was used to obtain a surface temperature distribution. The IR camera was TH7102 from NEC San-ei, and two optional lenses were attached to it to magnify an IR image. An IR temperature is affected by a window temperature, test section surface reflections and kinds of gases in an optical path. The window was cooled with room

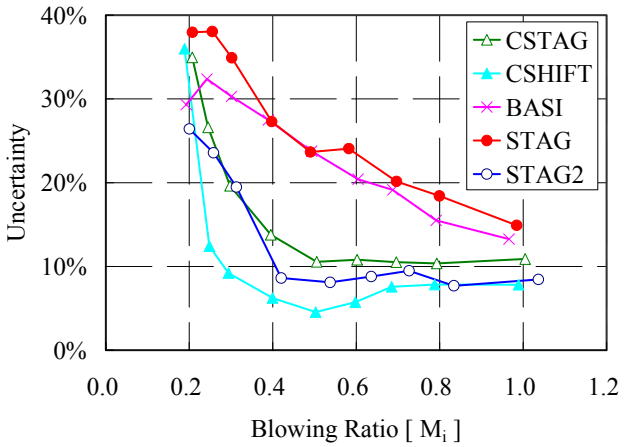

Figure 6 Uncertainties

temperature air. A temperature of a mixture of the window cooling air and the combustion gas was measured in front of the window. And it was in the range from 290K to 305K through all the experiments. Thus the window temperature is considered to be almost the same as the room temperature in all the experiments. Emissivety of a specimen surface painted with the black coat has been confirmed by a confirmation test. The confirmation test has been conducted in the wind tunnel rig with no combustion gas flow and heated cooling air flow to minimize conduction errors of thermocouple measurements for a calibration. The IR temperatures were compared with the temperatures measured by thermocouples embedded in a specimen. Constant emissivity has been confirmed in the temperature range that covers the surface temperatures observed in the cooling effectiveness test, and the value is 0.94. The gas temperature (T_g), the gas mass flow rate (W_g) and the fuel flow rate were set to almost the same value for all the experiments. Thus IR-ray absorption by the combustion gas is considered to be unchanged in all the experiments. The IR camera and a specimen were set at the same geometry in all the experiments. Thus view factors are also considered to be the same in all the experiments. The temperatures of circumferences are considered to be almost the same as the gas temperature, because circumferences are made of the low thermal conductivity material. Thus effects of reflections on the IR temperatures are considered to be almost the same in all the experiments, although the reflections are considered to be small because of the high emissivity of the specimen surfaces. As mentioned above, the conditions that affect the IR temperature are considered to be almost the same in all the experiments. Because the purpose of this study is a relative comparison of the local cooling effectiveness distribution, the IR temperature without the calibration is used to evaluate the cooling effectiveness distribution to avoid accounting conduction errors by the calibration using the thermocouples.

TEST CONDITIONS

Reynolds number of the combustion gas flow, Re_g, was set at 3.8×10^5. And Reynolds number of the cooling air flow, Re_c was varied from 5.0×10^3 to 3.0×10^4. Re_g is determined based on the velocity of the combustion gas flow

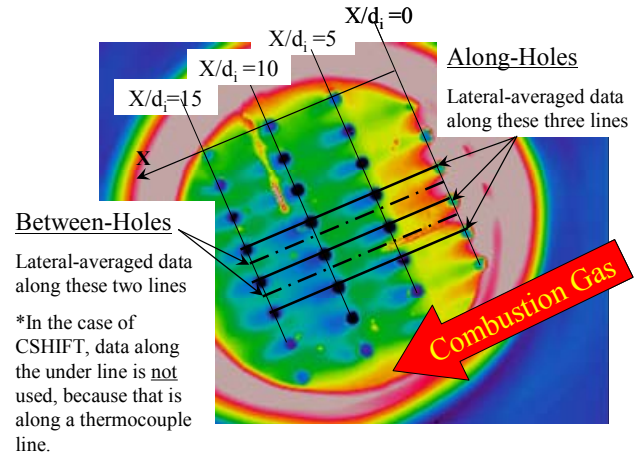

Figure 7 Lines where Local Cooling Effectiveness are Evaluated

and the specimen length along the combustion gas flow direction. And T_g is a reference temperature in evaluating the physical properties of the combustion gas. Re_c is determined based on the velocity of the impingement jet and the diameter of the impingement hole. And $T_{c,in}$ is a reference temperature in evaluating physical properties of the cooling air. Temperatures of the combustion gas and the cooling air were set lower than an actual engine condition to minimize a measurement error. The gas temperature was 673K. A density ratio of the cooling air to the combustion gas could be set about 2.0 as the same level as an actual engine condition without a use of the electric heater. However it was difficult to prevent the cooling air from heating by the thermal conduction. Thus the cooling air temperature at the inlet of the specimen varied from 290K to 370K depending on an amount of cooling air flow. Consequently the density ratio of the cooling air to the combustion gas varied from 1.5 to 2.2, although it was not intended. Because a cooling air temperature rise increases with decreasing an amount of cooling air flow, the density ratio decreases with decreasing an amount of cooling air flow.

UNCERTAINTY

Cooling effectiveness is evaluated in this study. It is defined as

$$\eta = \frac{T_g - T_{w,g}}{T_g - T_{c,in}} \tag{2}$$

The uncertainties for 95% confidence in obtained cooling effectiveness are estimated and shown in Figure 6. These uncertainties are mainly caused by high biases of the cooling air inlet temperature ($T_{c,in}$) originated from a temperature distribution of $T_{c,in}$. The smaller cooling air flow caused the larger temperature difference in the spatial distribution of $T_{c,in}$ because the local heating of the cooling air was easier to occur. Thus the uncertainties are high in the small blowing ratios.

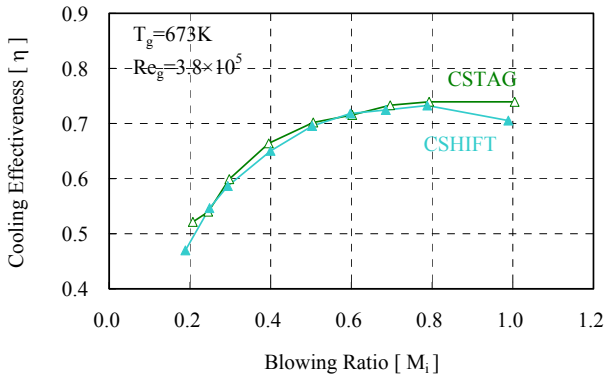

Cooling effectiveness vs. blowing ratio

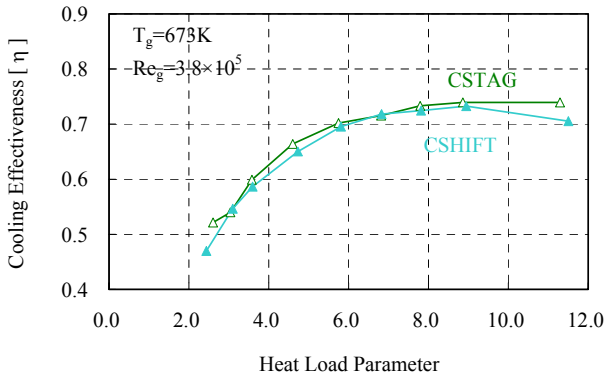

Cooling Effectiveness vs. Heat Load Parameter

Figure 8 Area-averaged cooling effectiveness of CSHIFT and CSTAG

RESULTS AND DISCUSSIONS

Figure 7 shows an example of the IR images, and explains where local cooling effectiveness is evaluated. Two local cooling effectiveness, "Along-Holes" and "Between-Holes" are evaluated. Along-Holes is representing a local cooling effectiveness distribution along a line that is run through the centers of film cooling holes in X direction. Along-Holes data are obtained by averaging three data that are obtained at the same X/d_i and different three Y/d_i locations. Between-Holes is representing local cooling effectiveness along a line between the film cooling holes in X direction. Between-Holes data are obtained by averaging two data that are obtained at the same X/d_i and different two Y/d_i locations, except for CSHIFT. In the case of CSHIFT, the data along one of two evaluation lines are not used because they are just along the thermocouple line. Thus Between-Holes data of CSHIFT are not averaged. The region of $0.0 < X/d_i < 5.0$ is near an edge of a specimen, so an inside flow may be out of a periodical condition. Thus local cooling effectiveness are evaluated in the region of $5.0 < X/d_i < 15.0$.

(1) Hole arrangement effect (CSHIFT and CSTAG)

CSHIFT and CSTAG are the specimens without pin. They are different in the relative location of a film cooling hole to the nearest impingement hole. An influence of a hole

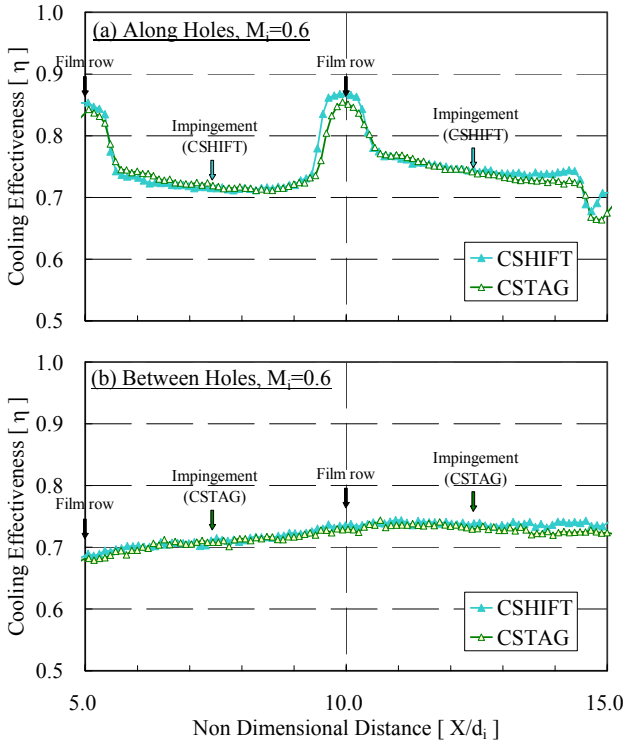

Figure 9 Local cooling effectiveness of CSHIFT and CSTAG at M_i=0.6

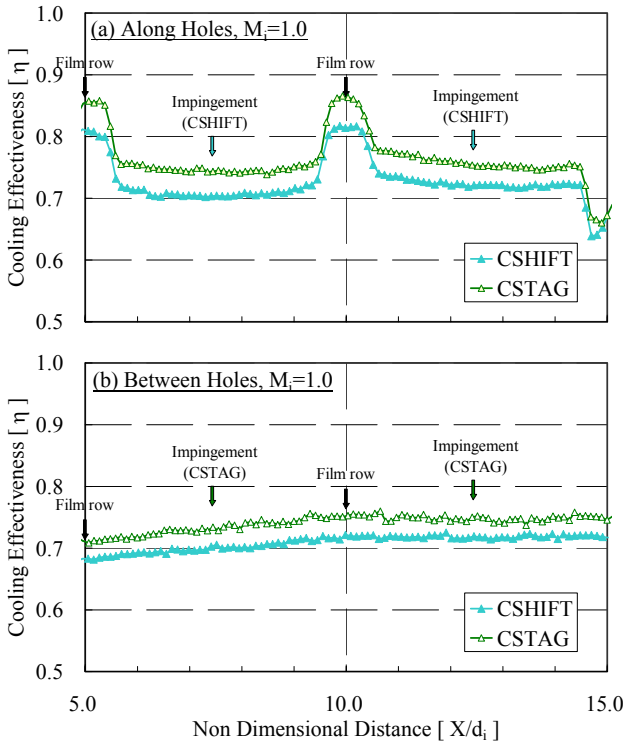

Figure 10 Local cooling effectiveness of CSHIFT and CSTAG at M_i=1.0

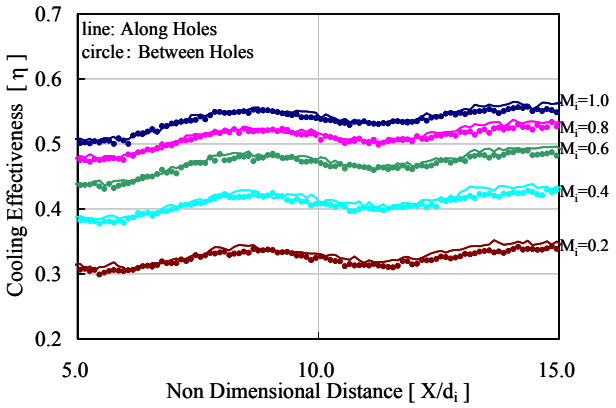

Figure 11 Local cooling effectiveness of REF

arrangement on cooling effectiveness is discussed in this section.

The area-averaged cooling effectiveness data of CSHIFT and CSTAG are shown in Figure 8. Figure 8 (a) and (b) show the area-averaged cooling effectiveness data as functions of blowing ratio (M_i) and the heat load parameter (HLP), respectively. HLP is defined as below.

$$HLP = \frac{Cp_c \times W_c}{A_{surf} \times h_g} \tag{3}$$

Combustion gas conditions are set almost the same for each test. Thus the parameters concerned with the gas conditions or gas side heat transfer conditions are almost constant for every cooling air condition and for every specimen test. Although a cooling air temperature depends on cooling air mass flow rate, the influence of the variation of the cooling air temperature is negligible in M_i and HLP. Thus both of M_i and HLP are considered functions of the cooling air mass flow rate. Consequently the shapes of cooling effectiveness curves in Figure 8 (a) and (b) are not influenced by variables (parameters of horizontal axis). However it is considered that showing the cooling effectiveness as a function of HLP helps an understanding the results. Thus Figure 8 (b) is set.

The area-averaged cooling effectiveness of CSHIFT and CSTAG are almost the same except the data at M_i=1.0.

Local cooling effectiveness distributions at M_i=0.6 and M_i=1.0 are shown in Figure 9 and Figure 10 respectively. The horizontal axis and the vertical axis in the figures indicate non-dimensional distance from the first film cooling row along the combustion gas flow direction (See Figure 7) and the local cooling effectiveness defined by Equation (2), respectively. Figure 9 shows that there is no difference between the local cooling effectiveness distributions of CSHIFT and CSTAG, although CSHIFT and CSTAG are different in the relative location of a film cooling hole to the nearest impingement cooling hole. Biot number under the experimental condition was about 0.2. Thus it is considered that a temperature distribution on the coolant side surface of the target plate is leveled and observed on the combustion gas side surface of the target plate. To confirm this assumption, local cooling effectiveness distributions of REF are evaluated. The results are shown in Figure 11. Figure 11 shows that there is no difference between local cooling effectiveness Along-Holes(along impingement holes) and that on Between-Holes(between impingement holes). Thus it is confirmed the assumption.

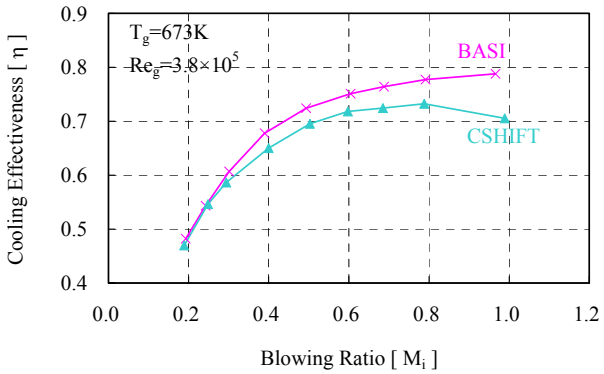

(a) Cooling effectiveness vs. blowing ratio

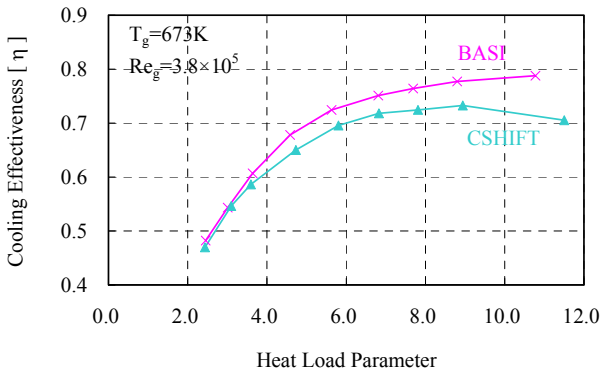

Cooling effectiveness vs. heat load parameter

Figure 12 Area-averaged cooling effectiveness of CSHIFT and BASI

Local cooling effectiveness distributions of CSHIFT and CSTAG at M_i=1.0 are shown in Figure 10. The shapes of the distributions of CSTAG and CSHIFT are almost the same though the absolute value of cooling effectiveness of CSTAG and CSHIFT are different. It is clarified that the difference between area-averaged cooling effectiveness of CSHIFT and CSTAG is not due to the difference between the shapes of the local cooling effectiveness distributions of CSHIFT and CSTAG. The reason why the absolute value of cooling effectiveness of CSHIFT and CSTAG are different should be investigated. Now, the reason is supposed that the film cooling effectiveness may be different because flow field inside the specimen may be affected by the arrangement of holes.

(2) Pin additional effect 1 (CSHIFT and BASI)

The pin effect on the cooling effectiveness is confirmed by comparing the results of CSHIFT and BASI. CSHIFT and BASI have the same hole arrangement. The difference between them is that pins exist or not.

The area-averaged cooling effectiveness curves are shown in Figure 12. As same as Figure 8, the area-averaged cooling effectiveness data are shown as functions of blowing ratio (M_i) and the heat load parameter (HLP) in Figure 12. Although the area-averaged cooling effectiveness of CSHIFT and BASI are almost the same in the region of $M_i < 0.25$, the area-averaged cooling effectiveness of BASI is higher than that

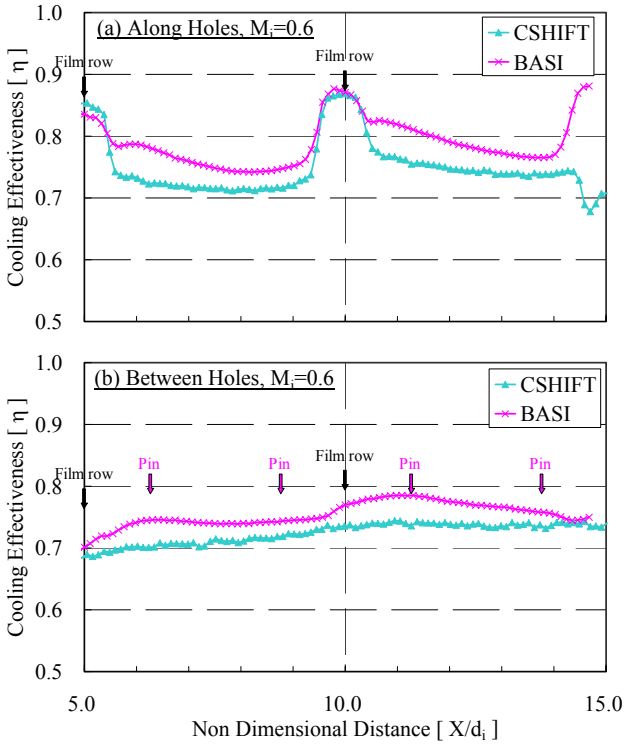

Figure 13 Local cooling effectiveness of CSHIFT and BASI at M_i=0.6

of CSHIFT in the higher M_i region, and the advantage of BASI increases with increasing M_i.

The local cooling effectiveness distributions of CSHIFT and BASI at M_i=0.6 are shown in Figure 13. BASI shows higher cooling effectiveness in whole locations. It is supposed that the improvement is due to a pin effect. The shapes of the local cooling effectiveness distributions of BASI are different from those of CSHIFT.

At first, the cooling effectiveness improvement at the exact locations of the pins is discussed. The locations of pins are indicated in the figure. Two pins are arranged in the unit area of BASI, as shown in Table 1. The local cooling effectiveness in the two unit area from the second film cooling hole row to the fourth film cooling hole row are shown in Figure 13. Thus four pins are indicated in Figure 13 (b). Figure 13 (b) shows that the cooling effectiveness improvement of BASI to CSHIFT is remarkable at the pin locations of X/d_i=6.25 and 11.25. Those locations are the upstream side pin locations in the unit area. On the other hand, the local cooling effectiveness of BASI at the pin locations of X/d_i=8.75 and 13.75 are not much improved to those of CSHIFT. The locations of X/d_i=8.75 and 13.75 are the downstream side pin locations in the unit area. Four film cooling hole rows and four impingement hole rows exist in each specimen. And the first film cooling hole row is located upstream to the first impingement hole row. Thus it is considered that the cooling air tends to flow out from the upstream side film cooling hole. So it is considered that the flow rate of the cooling air that flows to the upstream side film cooling hole from the impingement hole is more than the flow rate of the cooling air that flows to the downstream side film cooling hole from the impingement hole.

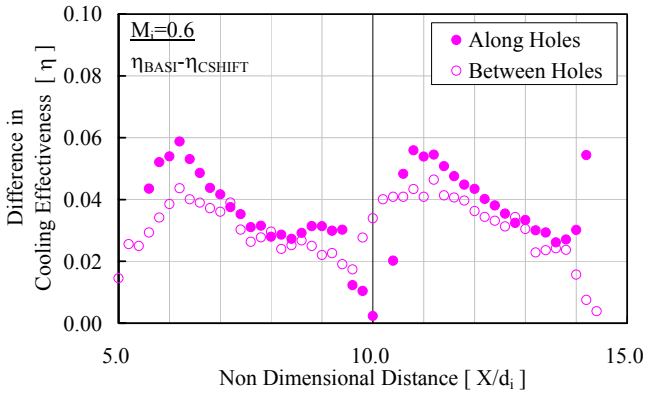

Figure 14 Difference in cooling effectiveness between CSHIFT and BASI at M_i=0.6

This asymmetry of the flow field may be a cause that a pin effect on the local cooling effectiveness depends on its location.

Next, Along-Holes data of the local cooling effectiveness (shown in Figure 13 (a)) are discussed. There is no pin along the evaluation lines of Along-Holes in BASI. Thus, there is no difference in the cooling configuration between BASI and CSHIFT along the evaluation lines of Along-Holes. However as shown in Figure 13 (a), the local cooling effectiveness are different. The advantage of BASI is largest immediately after film cooling holes. And the advantage of BASI decreases as X/d_i increases.

Figure 14 shows remainders that are subtracted the local cooling effectiveness of CSHIFT from that of BASI. In the figure, the regions of $5.0<X/d_i<5.5$, $9.5<X/d_i<10.5$ and $14.5<X/d_i<15.0$ in Along-Holes plots correspond to a film cooling hole. Thus, the data in these regions are no meaning. The figure shows that the improvement in the cooling effectiveness is the largest just after a film cooling hole. This result is worth paying an attention because the improvement in the cooling effectiveness is the largest though there is no difference between the configurations of CSHIFT and BASI along the evaluation lines of Along-Holes. Along-Holes data and Between-Holes data are almost the same in the downstream half of the unit area. As mentioned before, a temperature distribution on the coolant side surface of the target plate is leveled and observed on the combustion gas side surface of the target plate in the test condition. This is considered to be the reason that Along-Holes data and Between-Holes data are almost the same in the downstream half of the unit area. Because the largest improvement just after a film cooling hole is observed very locally, film cooling effectiveness of BASI may be different from that of CSHIFT and different film cooling effectiveness may cause the local cooling effectiveness differences. It is considered that the film cooling effectiveness may be different because flow fields inside the specimens may be affected by the existence of pins.

(3) Pin additional effect 2 (CSTAG, STAG and STAG2)

The area-averaged cooling effectiveness of CSTAG, STAG and STAG2 are shown in Figure 15. Figure 15 (a) and (b) show the area-averaged cooling effectiveness data as functions of blowing ratio (M_i) and the heat load parameter (HLP), respectively. The area-averaged cooling effectiveness of

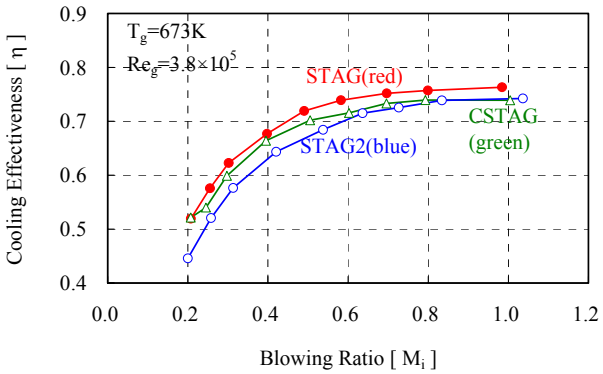

(a) Cooling effectiveness vs. blowing ratio

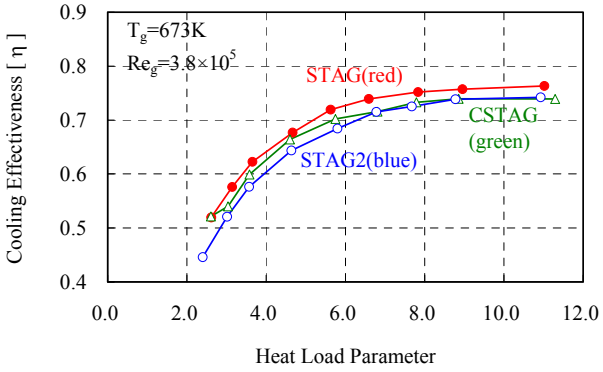

(b) Cooling effectiveness vs. heat load parameter

Figure 15 Area-averaged cooling effectiveness of CSTAG, STAG and STAG2

STAG is higher than that of STAG2 in the whole M_i region, although they have the same pin density.

Local cooling effectiveness at M_i=0.6 are shown in Figure 16. Figure 16 (a) shows Along-Holes data of local cooling effectiveness distributions. The improvement in the local cooling effectiveness of STAG to CSTAG looks constant and independent of a location, except that the distribution of STAG waves weakly as it becomes convex at the pin locations. In the Along-Holes data of STAG, there exist the data that are lower than the data around in the range of $10.5<X/d_i<11.0$. This is caused by a material defect, thus it is not essential. The local cooling effectiveness distribution of STAG2 is the most different from the others. The local cooling effectiveness of STAG2 is as high as that of STAG just after a film cooling hole, but it decreases rapidly as X/d_i increases. And finally it falls in the level of the cooling effectiveness of CSTAG. There exists no indication of the existence of the pins in the local cooling effectiveness distribution of STAG2.

Figure 16 (b) shows Between-Holes data of the local cooling effectiveness. The local cooling effectiveness of STAG is higher than that of CSTAG in a broad region after a pin location. The advantage decreases toward the following pin location. Although the difference between the local cooling effectiveness distributions of CSTAG and STAG2 is not clear in Figure 16 (b), that appears more clearly in the less cooling air conditions.

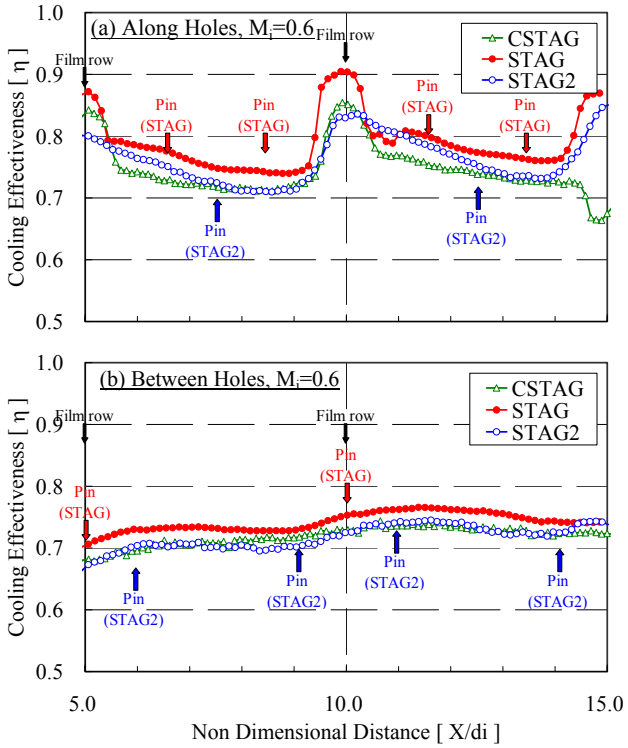

Figure 16 Local cooling effectiveness of CSTAG, STAG and STAG2 at M_i=0.6

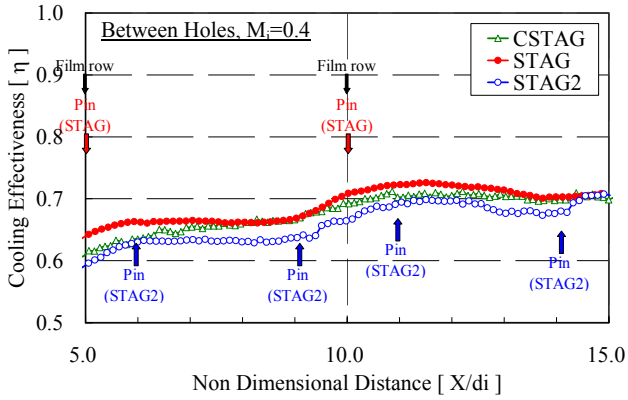

Figure 17 Local cooling effectiveness of CSTAG, STAG and STAG2 at M_i=0.4

Thus Between-Holes data of local cooling effectiveness at M_i=0.4 are shown in Figure 17. The local cooling effectiveness of STAG2 is lower than that of CSTAG, although STAG2 has pins to enhance the cooling performance along the lines that Between-Holes data are evaluated. The local cooling effectiveness of STAG2 at the pin locations of X/d_i=5.94 and 10.94 are only data as high as the data of CSTAG, although the local cooling effectiveness data of SATG2 are lower than those of CSTAG at the remaining locations. X/d_i=5.94 and 10.94 are the upstream side pin

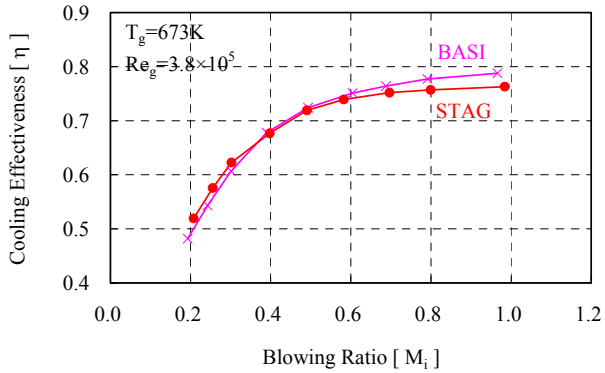

(a) Cooling effectiveness vs. blowing ratio

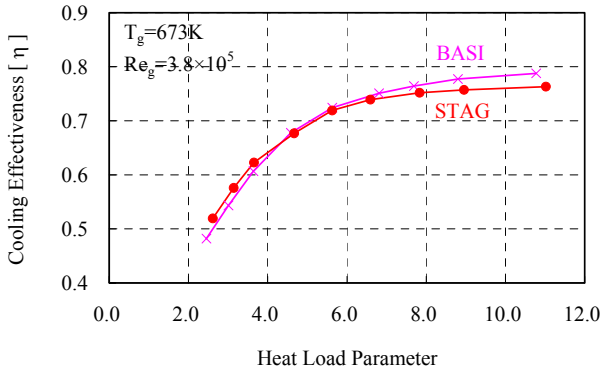

(b) Cooling effectiveness vs. heat load parameter

Figure 18 Area-averaged cooling effectiveness of BASI and STAG

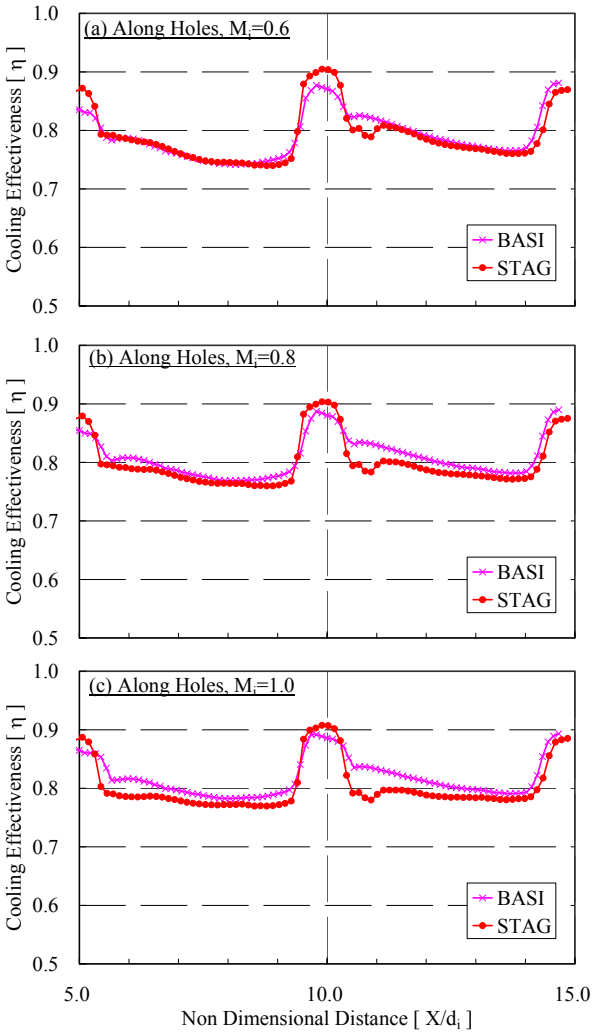

Figure 19 Local cooling effectiveness along holes of BASI and STAG

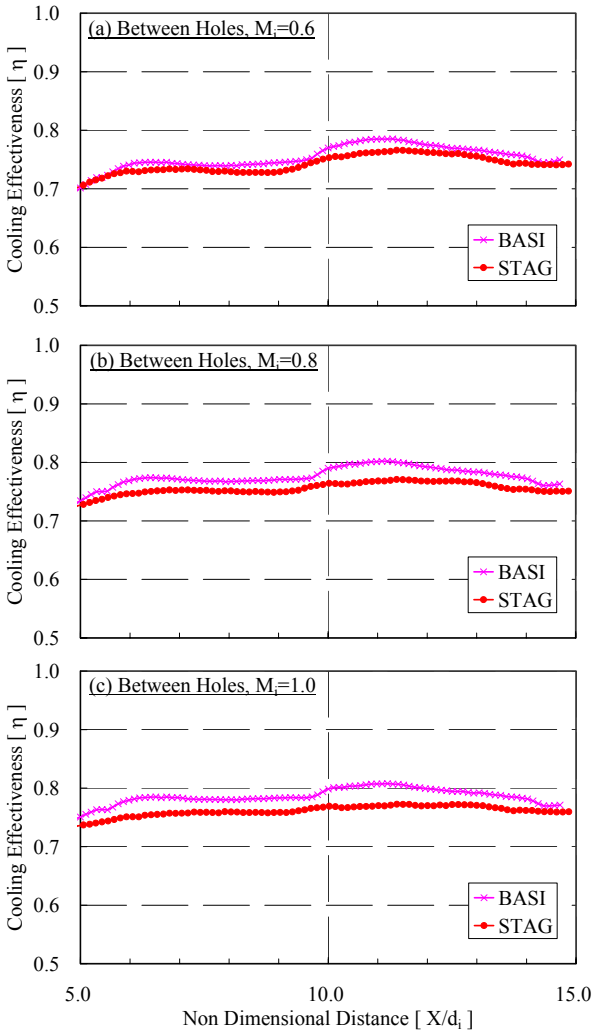

Figure 20 Local cooling effectiveness between holes of BASI and STAG

locations in the unit area. On the other hand, the local cooling effectiveness of STAG2 at the pin locations of X/d_i=9.06 and 14.06 where are the downstream side pin locations are not much improved. Thus a pin effect on the local cooling effectiveness of STAG2 also depends on its location as same as the case of BASI, as mentioned in clause (2) in this section (See Figure 13). This is also considered that it may be caused by the asymmetry of the flow field, as mentioned in clause (2) in this section.

In the local cooling effectiveness distributions of STAG and STAG2, the effects of the pins appear more locally than the pin effect that is observed in BASI (See Figure 13). One of the reasons is considered that pins in STAG and STAG2 are smaller in diameter than pins in BASI.

(4) Pin arrangement effect (BASI and STAG)

The area-averaged cooling effectiveness curves of BASI and STAG are shown in Figure 18. The area-averaged cooling effectiveness data are shown as functions of blowing ratio (M_i) and the heat load parameter (HLP) in Figure 18. The area-averaged cooling effectiveness of BASI and STAG are almost the same in the region of $M_i < 0.5$. However the area-averaged cooling effectiveness of BASI is higher than that of STAG in the higher M_i region, and an advantage of the area-averaged cooling effectiveness of BASI to STAG increases as M_i increases.

The local cooling effectiveness distributions of BASI and STAG are shown in Figure 19 and Figure 20. Figure 19 shows Along-Holes data. The local cooling effectiveness distributions of BASI and STAG are almost the same at M_i =0.6 (Figure 19 (a)). However distribution shapes in the higher M_i region are different. Although the distribution shapes of BASI do not depend on M_i, the distribution shapes of STAG change by M_i as a decreasing rate of the local cooling effectiveness to the X/d_i increase in the downstream region of a film cooling hole decreases with an increase of M_i. Thus the local cooling effectiveness distributions from a film cooling hole to the next film cooling hole becomes flat as M_i increases. Consequently the advantage of BASI in the local cooling effectiveness to STAG is the largest just after a film cooling hole, and it decreases with the X/d_i increase. This shows that the improvement of the local cooling effectiveness of STAG at the pin locations (X/d_i=6.56, 8.43, 11.56 and 13.43) diminishes with the M_i increase. On the other hand, even though there is no pin in BASI along the line that Along-Holes data are evaluated, the pin effect is shown. And the effect continues in higher M_i conditions.

Figure 20 shows Between-Holes data. The local cooling effectiveness of BASI is higher than that of STAG at the exact location of the pins in BASI (X/d_i=6.25 and 11.25). This shows that the pins in BASI work effectively than the pins in STAG. The dependencies of the local cooling effectiveness distribution shapes of BASI and STAG on M_i resemble the results of Along-Holes shown in Figure 19. Thus an advantage of BASI in the local cooling effectiveness to STAG increases with the M_i increase. However the largest advantage is observed still at the exact location of the pins in BASI (X/d_i=6.25 and 11.25). As same as the results of Along-Holes in Figure 19, the pin benefit in STAG diminishes with increasing M_i while the pin benefit in BASI continues to exist at the higher M_i values.

CONCLUSIONS

To obtain a better knowledge about a pin/hole arrangement effect on cooling effectiveness, local cooling effectiveness distributions have been newly evaluated to the existing experimental data that were obtained through the study carried out by Nakamata et al. [5]. The present paper first describes the detailed local cooling effectiveness for the several cooling configurations that have the different pin/hole arrangements to clarify an influence of pin/hole arrangements on cooling effectiveness. Followings are important findings obtained through the present study.

(1) A hole arrangement effect on a local cooling effectiveness distribution has been evaluated. Two specimens that have different hole arrangements and no pin are tested. They are CSHIFT and CSTAG. A relative location of a film cooling hole to the nearest impingement hole is the difference between the two specimens. There is no difference between the local cooling effectiveness distributions of CSHIFT and CSTAG. It is considered that the temperature distribution on the coolant side surface of the target plate is leveled and observed on the combustion gas side surface of the target plate because of the low Biot number of the test conditions.
(2) A pin additional effect on a local cooling effectiveness distribution has been evaluated to three different configurations. BASI, STAG and STAG2 are tested. The pin additional effect has been clarified by comparing the results obtained from the specimens with and without pins. The followings are observed commonly for all three configurations with pins. The cooling effectiveness improvement of the configuration with pins to the configuration without pin is remarkable at the upstream side pin locations in the unit area. On the other hand, the cooling effectiveness of the configuration with pins is not much improved to the configuration without pin at the downstream side pin locations in the unit area. This is considered that it may be caused by the asymmetry of the flow field.
(3) A pin arrangement effect has been evaluated by comparing the results of BASI and STAG. The pins in BASI work more effectively than the pins in STAG. The pin benefit in STAG diminishes with increasing M_i while the pin benefit in BASI continues to exist at the higher M_i values.

ACKNOWLEDGMENTS

The authors would like to express their thanks to the New Energy and Industrial Technology Development Organization (NEDO) and the Ministry of Economy, Trade and Industry (METI), who gave them the opportunity to conduct "Research and Development of Environmentally Compatible Propulsion System for Next-Generation Supersonic Transport (ESPR) project".

REFERENCES

1. Gillespie, D. R. H., Wang, Z., Ireland, P. T. and Kohler, S. T., 1996, “Full Surface Local Heat Transfer Coefficient Measurements in a Model of an Integrally Cast Impingement Cooling Geometry,” ASME Paper 96-GT-200

2. Sweeney, P. C. and Rhodes, J. F., 1999, "An Infrared Technique for Evaluating Turbine Airfoil Cooling Designs", ASME Paper 99-GT-142

3. Taslim, M. E., Setayeshgar, L., and Spring, S. D., 2000, "An Experimental Evaluation of Advanced Leading Edge Impingement Cooling Concepts", ASME Paper 2000-GT-0222

4. Funazaki, K., Tarukawa, Y., Kudo, T., Matsuno, S., Imai, R. and Yamawaki, S., 2001, "Heat Transfer Characteristics of an Integrated Cooling Configuration for Ultra-High Temperature Turbine Blades: Experimental and Numerical Investigations", ASME Paper 2001-GT-148

5. Nakamata, C., Okita, Y., Matsuno, S., Mimura, F., Matsushita, M., Yamane, T., Fukuyama, Y., Yoshida, T., 2005, "Spatial Arrangement Dependence of Cooling Performance of an Integrated Impingement and Pin Fin Cooling Configuration", ASME paper GT2005-68348

6. Zhang, C., Xu, Q., Zhao, M., Lin, Y., Liu, G., 2006, "Effect of Impingement/Effusion Hole-Area Ratio on Discharge Coefficients of Double Cooling Wall", ASME Paper GT2006-90612

7. Bunker, R. S., Bailey, J. C., Lee, C. P. and Stevens, C. W., 2004, "In-Wall Network (Mesh) Cooling Augmentation of Gas Turbine Airfoils", ASME Paper GT2004-54260

8. Trabold, T. A. and Obot, N. T., 1987, "Impingement Heat Transfer within Arrays of Circular Jets. Part II: Effects of Crossflow in the Presence of Roughness Elements", ASME Paper 87-GT-200

9. Haiping, C., Dalin, Z. and Taiping H., 1997, "Impingement Heat Transfer from Rib Roughened Surface within Arrays of Circular Jets: The Effect of the Relative Position of the Jet Hole to the Ribs", ASME Paper 97-GT-331

10. Hoecker, R., Johnson, B.V., Hausladen, J., Rothbrust, M. and Weigand, B., 1999, "Impingement Cooling Experiments with Flat Plate and Pin Plate Target Surfaces", ASME Paper 99-GT-252

11. Annerfeldt, M. O., Persson, J. L., and Torisson, T., 2001, "Experimental Investigation of Impingement Cooling with Turbulators or Surface Enlarging Elements", ASME Paper 2001-GT-149.

12. Andrews, G. E., Abdul Hussain, R. A. A., and Mkpadi, M. C., 2004, "Enhanced Impingement Heat Transfer: the Influence of Impingement X/D for Interrupted Rib Obstacles (Rectangular Pin Fins)", ASME paper GT2004-54184

13. Andrews, G. E., Asere, A. A., Hussain, C. I., Mkpadi, M. C. and Nazari, A., 1988, "Impingement/Effusion Cooling: Overall Wall Heat Transfer", ASME Paper 88-GT-290

14. Al Dabagh, A. M., Andrews, G. E., Abdul Husain, R. A. A., Husain, C. I., Nazari, A. and Wu, J., 1989, "Impingement/Effusion Cooling: The Influence of the Number of Impingement Holes and Pressure Loss on the Heat Transfer Coefficient", ASME Paper 89-GT-188

15. Cho, H. H. and Rhee, D. H., 2001, "Local Heat/Mass Transfer Measurement on the Effusion Plate in Impingement/Effusion Cooling Systems," J. of Turbomachinery, **123**, pp. 601-608.

16. Cho, H. H., Rhee, D. H. and Goldstein, R. J., 2004, "Effects of Hole Arrangements on Local Heat/Mass Transfer for Impingement/Effusion Cooling with Small Hole Spacing", ASME Paper GT2004-53685

17. Yamawaki, S., Nakamata, C., Imai, R., Matsuno, S., Yoshida, T., Mimura, F., Kumada, M., 2003, "Cooling Performance of an Integrated Impingement and Pin Fin Cooling Configuration", ASME Paper GT2003-38215

18. Favaretto, C. F. F.and Funazaki, K., 2003, "Application of Genetic Algorithms to Design of an Internal Turbine Cooling System", ASME Paper GT2003-38408

19. Chambers, A. C., Gillespie, D. R. H., Ireland, P. T., Mitchell, M., 2006, "Enhancement of Impingement Cooling in a High Cross Flow Channel using Shaped Impingement Cooling Holes", ASME Paper GT2006-91229

20. Ieronymidis, I., Gillespie, D. R. H., Ireland, P. T., Kingston, R., 2006, "Detailed Heat Transfer Measurements in a Model of an Integrally Cast Cooling Passage", ASME Paper GT2006-91231

21. Ieronymidis, I., Gillespie, D. R. H., Ireland, P. T., Kingston, R., 2006, "The Use of High Blockage Ribs to Enhance Heat Transfer Coefficient Distributions in a Model of an Integrally Cast Cooling Manifold", ASME Paper GT2006-91237

22. Ieronymidis, I., Gillespie, D. R. H., Ireland, P. T., Kingston, R., 2006, "Experimental and Computational Flow Field Studies of an Integrally Cast Cooling Manifold with and without Rotation", ASME Paper GT2006-91245

23. Battisti, L., Fedrizzi, R., Cerri, G., 2006, "Novel Technology for Gas Turbine Blade Effusion Cooling", ASME Paper GT2006-90516

24. Coutandin, D., Taddei, S., Facchini, B., 2006, "Advanced Doublewall Cooling System Development for Turbine Vanes", ASME Paper GT2006-90784

